Journal of Magnetic Resonance 200 (2009) 81–87

Contents lists available at ScienceDirect

Journal of Magnetic Resonance

journal homepage: www.elsevier.com/locate/jmr

Cryogenic 35 GHz pulse ENDOR probehead accommodating large sample sizes: Performance and applications

René Tschaggelar [a], Besnik Kasumaj [a], Maria Grazia Santangelo [a], Jörg Forrer [a], Patrik Leger [a], Henry Dube [b,1], François Diederich [b], Jeffrey Harmer [a,2], Rolf Schuhmann [c], Inés García-Rubio [a,*], Gunnar Jeschke [a]

[a] Laboratory of Physical Chemistry, ETH Zurich, Zürich CH-8093, Switzerland
[b] Laboratory of Organic Chemistry, ETH Zurich, Zürich CH-8093, Switzerland
[c] Fachgebiet Theoretische Elektrotechnik, Universität Paderborn, 33098 Paderborn, Germany

ARTICLE INFO

Article history:
Received 31 December 2008
Revised 22 April 2009
Available online 12 June 2009

Keywords:
ENDOR
Pulse EPR
ENDOR resonator
Q-band probehead
Large sample resonator

ABSTRACT

The construction and performance of a cryogenic 35 GHz pulse electron nuclear double resonance (ENDOR) probehead for large samples is presented. The resonator is based on a rectangular TE_{102} cavity in which the radio frequency (rf) B_2-field is generated by a two turn saddle ENDOR coil crossing the resonator along the sample axis with minimal distance to the sample tube. An rf power efficiency factor is used to define the B_2-field strength per square-root of the transmitted rf power over the frequency range 2–180 MHz. The distributions of the microwave B_1- and E_1-field, and the rf B_2-field are investigated by electromagnetic field calculations. All dielectrics, the sample tube, and coupling elements are included in the calculations. The application range of the probehead and the advantages of using large sample sizes are demonstrated and discussed on a number of paramagnetic samples containing transition metal ions.

1. Introduction

ENDOR is an important branch of pulse electron paramagnetic resonance (EPR) and a versatile spectroscopic tool for the determination of electronic and geometric structures of paramagnetic species. Pulse ENDOR spectroscopy [1,2] as compared to continuous wave (cw) ENDOR [3,4] has some advantages, the ENDOR efficiency can be up to 100%, leading to higher ENDOR signal intensities than in the cw approach [5,6], it is less dependent on the balance of relaxation rates and the spectra are measured in absorption mode. Moreover, pulse ENDOR spectra are less susceptible to baseline distortions, particularly if stochastic excitation is used [7–9].

Pulse ENDOR spectrometers and probeheads have been developed for a broad range of frequencies. For many applications ENDOR in the 33–36 GHz frequency range (Q-band) is the experiment of choice because of the improved nuclear Zeeman spectral resolution, the reduced broadening and asymmetries due to second-order effects, and the improved orientation selectivity of the microwave (mw) pulses as compared to X-band frequencies of about 9.6 GHz. In addition, when going to higher excitation frequencies strong-level mixing is usually reduced, consequently, the ENDOR effect is enhanced and the ESEEM effect is reduced, i.e. the impacts of cross-suppression and implicit triple [10,11] are decreased. Compared to ENDOR at even higher frequencies, Q-band pulse ENDOR has substantially better concentration sensitivity.

Recently we showed that the application of loop-gap resonators (LGR) at 35 GHz with high filling factors, matched for particular sample sizes, lead to optimum mw B_1-field strengths in the sample area [12]. It has also been shown that strong electron spin echo (ESE) signals are generated at 35 GHz resonance frequencies using large sample sizes with TE_{011} cylindrical cavities [8,13–15]. This feature is important for samples with low concentration of the paramagnetic centers where the echo amplitude only slightly exceeds the noise level of the receiver. Additionally, the use of oversized samples at Q-band allows using the same sample tubes as at X-band with LGR and dielectric ring (DR) resonators. This is a further advantage, which is especially important when dealing with very rare and precious samples or when preparation steps, such as a gas exchange, require considerable effort.

Rectangular resonant cavities [16] as the one described in this work have been widely used for cw ENDOR measurements [17,18] since this technique was introduced [19] and the first commercial EPR spectrometers became available [20]. Later they were also applied for ESE experiments. As compared to the LGR and DR-ENDOR resonators [21,22], a TE_{102} resonant cavity has a much lower pulse power efficiency, $\Lambda_{p(mw)}$ (magnetic field of the mw pulse

* Corresponding author. Fax: +41 44 632 1021.
E-mail address: garciarubio@phys.chem.ethz.ch (I. García-Rubio).
[1] Present address: The Scripps Research Institute, San Diego, USA.
[2] Present address: University of Oxford, UK.

1090-7807/$ - see front matter © 2009 Elsevier Inc. All rights reserved.
doi:10.1016/j.jmr.2009.06.007

for a given mw power) but it allows for larger sample volumes. As compared to the cylindrical TE_{011} resonant cavities, a TE_{102} resonant cavity has a lower signal efficiency, Λ_{rs} (echo intensity for a given sample volume) however, it has a much smaller volume, which grants a higher filling factor. The ENDOR coil in the TE_{102} resonant cavity reduces the loaded quality factors Q_L from 700 to a suitable value between 200 and 400 in the frequency range 34–36 GHz. In contrast to the cylindrical cavity, there are no crossing modes appearing over this frequency range and, in our hands, it is easier to couple and overcouple. Practical cavity size and the ease of construction are other advantageous properties of the TE_{102} resonant cavity for pulse ENDOR applications at Q-band. Here we show the construction and performance of a 34–36 GHz broadband pulse ENDOR probehead equipped with a rectangular TE_{102} resonant cavity suitable for large sample sizes up to a diameter of 2.9 mm. This design leads to larger ESE amplitudes and improved ENDOR signal intensities for a given spin concentration, moreover, it allows the same sample to be used for 9 and 35 GHz pulse ENDOR measurements.

2. Probehead design

The probehead is designed to allow access to sample tubes of up to 2.9 mm diameter and to work from room to liquid helium temperatures in our Q-band spectrometer [23] equipped with a continuous He flow cryostat from Oxford Instruments (UK), The mw power is directed through a WR 28 waveguide into the TE_{102} ENDOR resonant cavity. The sample tube is placed in the center of the cavity, and is surrounded by a rf coil that generates the B_2-field. The resonance frequency of the empty cavity is higher than the spectrometer frequency range of 34–36 GHz and is shifted by the quartz sample tube ($\varepsilon = 4.2$) into the operating frequency range. Therefore, no frequency tuning is required.

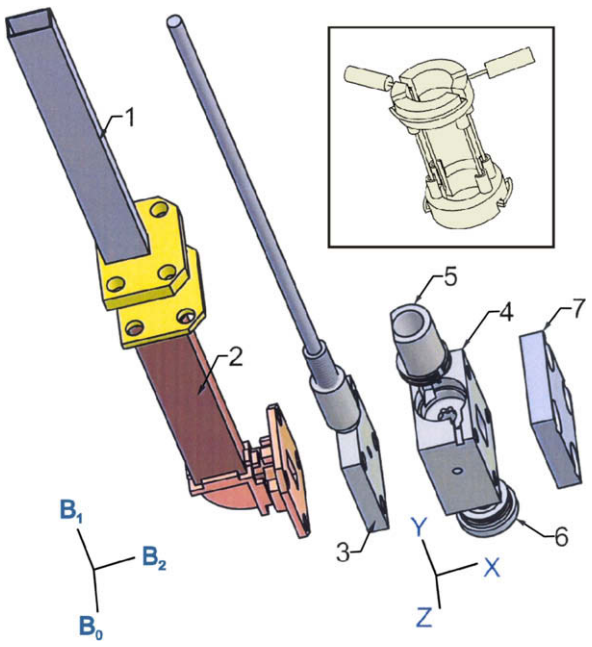

Fig. 1. Schematic drawing of the lower part of the ENDOR probehead. Stainless steel (1) and copper (2) WR 28 wave guide sections, (3) iris-coupler plate, (4) resonant cavity block, (5) sample feed, (6) bottom cover with hole for sample tube, (7) cover copper plate. On the lower part of the figure the directions of the different magnetic fields are shown together with the reference frame. The inset on the right upper side of the figure shows the wires and support that form the ENDOR coil. The whole construct is positioned along the y-axis in the cavity block (4).

The lower part of the probehead is shown in Fig. 1 in an expanded view. The TE_{102} ENDOR resonant cavity consists of a WR 28 wave guide section cut in an aluminum block (number 4, inner dimensions $10.1 \times 7 \times 5$ mm using the frame (x, y, z) shown in Fig. 1) that is terminated on both sides. On one side the ending is a 2 mm thick copper plate (7) and on the opposite side, a 3 mm iris-coupler plate (3) also made of copper. Inside the cavity space some of the edges were rounded (see Fig. 3 for the shape details of the cavity). All three parts of the resonator (aluminum block, cover plate and iris-coupler plate) are coated with 2 μm of silver (Collini-Flühmann AG, 8600 Dübendorf, Switzerland) and have the outside dimensions of the WR 28 flange. The iris-coupler plate, whose construction is detailed in reference [12], terminates the wave guide (2) in a $2.8 \times 7.0 \times 3.0$ mm round-shaped groove that has been carved in the plate. The groove is opened in the middle to the resonator space through a 3×1 mm slot along the y-axis (iris). Inside this groove, the tuning rod can move along the y-axis allowing the iris to be remotely tuned. The bottom cover (6) prevents mw leakage and has a hole in the middle that centers the sample and allows the He-gas flow.

The lower section of the wave guide (2) and the cast H-bend (MDL, type 28BE11B) that is connected to the iris-coupler plate are made from copper. The upper part of the WR 28 wave guide (1) is made of stainless steel coated with silver inside, it serves as a temperature barrier and connects to the upper part of the probehead. The sample tube is guided with a sample tube holder through the 12×8 mm i.d. epoxy sample access tube (not shown) via the sample feed, an aluminum intersection (5) with a 8–3.2 mm diameter reduction to the cavity block (4). This intersection guides the sample tube in the entrance of the ENDOR cavity, allows sample exchange at all temperatures, connects the sample access tube with the cavity block and adds additional mechanical stability.

The broadband rf excitation [24,25] in the sample is generated by four 0.25 mm diameter Teflon-insulated silver wires positioned along the sample axis (y-axis) that go through the resonator forming a two turn saddle ENDOR coil (the wire distances are 1.5 mm in the x- and 3.2 mm in the z-axis, see inset in Fig. 1). The four wires are spanned over two Teflon holders on the top and on the bottom of the cavity block, placing the wires very close to the 2.9 mm sample tube. In the upper part of the aluminum block, outside the resonant cavity, the ends of the coil are connected in series to the inner conductors of two copper coaxial cables while the outer conductors are connected to the aluminum block by pressing them into the grooves carved in its upper face. To and through the flange of the upper part of the probehead, the rf signal is conducted by stainless steel semi-rigid coaxial cables. Outside the cryostat, one of the two coaxial cables is connected to the rf supply, the rf amplifier (model: Amplifier Research 500A100A), the other one to a terminating 50 Ω/10 W load.

3. Electron spin echo and ENDOR performance

In this section we examine properties which characterize the mw B_1-field and the rf B_2-field of the TE_{102} ENDOR resonant cavity at room and cryogenic (20 K) temperatures. To probe the mw B_1-field, we measured the primary ESE following the Hahn sequence ($\pi/2$-τ-π-τ-ESE) with nominal pulse lengths of $t_{\pi/2} = 80$ ns and $t_\pi = 160$ ns and a free evolution time of $\tau = 300$ ns. The primary ESE is also used as the detection sub-sequence in the Davies ENDOR experiment, π_{mw}-π_{rf}-$\pi/2_{mw}$-τ-π_{mw}-τ-ESE, where the frequency of the rf pulse is varied. Davies ENDOR reflects the influence of an rf-inversion pulse on the spin system under investigation, and therefore it serves as probe for the rf B_2-field in the TE_{102} cavity, just as the primary ESE serves as probe for the mw

B_1-field performance. For all the experiments described in this section, the static magnetic field B_0 was set to the maximum of the EPR absorption line of either Pittsburgh coal at room temperature or a solution of $^{63}Cu(Gly)_2$ at 20 K. The optimum length of the rf pulse was found to be about 8500 ns using an rf-ENDOR nutation experiment.

The ESE and ENDOR signals were measured for three different sample sizes. For that, cylindrical quartz tubes with lengths of 7 mm and diameters (inner diameter (i.d.) × outer diameter (o.d.), in mm) 1.0 × 1.6, 1.5 × 1.8 and 2.5 × 2.9 were used. The smallest quartz tube (1.0 × 1.6 mm) was placed in an outer 2.5 × 2.9 mm quartz tube to shift the resonance frequency into the operating frequency range of our spectrometer. The same 1.0 × 1.6 mm tube was used without the outer tube to perform the same measurements with a commercial DR-ENDOR resonator (Bruker Biospin).

The room temperature performance of the TE_{102} ENDOR rectangular cavity is summarized in Table 1. For all sample sizes the loaded Q-factor was found to be in the range Q_L = 200–400. The second column of the table shows that along with an increase of the sample volume an increase of the primary ESE amplitude is observed, which is expected due to an increase of the filling factor. However, the increment is not linear with respect to the sample volume. This comparison is better made in terms of the resonator sensitivity factor (Λ_{rs}), which defines the ratio between the maximum ESE amplitude and the sample volume. The lower sensitivity factor of the bigger samples with respect to the 1.0 mm i.d. sample can be attributed to the larger volume of the first, which results in a more heterogeneous B_1-field and more dielectric losses in the sample volume. The sensitivity factors Λ_{rs} for the TE_{102} cavity are smaller than for the commercial dielectric ENDOR resonator for all sample sizes. This means that the commercial DR shows a better performance if the available sample amount is too small to fill an oversized tube. If a sufficient amount of sample is available, the ESE amplitude is significantly improved by the use of larger sample tubes because of the larger amount of spin centers that can contribute to the signal. This improvement is observed in spite of a reduced filling factor as compared to the DR.

The mw pulse power efficiency, $\Lambda_{p(mw)}$, is the ratio between the B_1-field strength of the mw pulse and the square-root of the applied mw power P_1. It is therefore a measure for the efficiency of the conversion from mw pulse power to effective B_1-field strength. The mw pulse power efficiency $\Lambda_{p(mw)}$ of our resonator is approximately the same for all sample sizes but significantly less than the one of the DR-ENDOR resonator (see Table 1) and consequently higher mw power is required to flip the electron spins. This result underlines that the significant signal gain at given concentration in our TE_{102} resonator is reached at the cost of absolute sensitivity and mw pulse power efficiency.

The ENDOR peak amplitudes were measured at the proton Larmor frequency, 51 MHz approximately. The noise level in the spectra was estimated at about 66 MHz (15 MHz away from the main ENDOR transition) and it was found to be approximately the same for all sample sizes. Therefore, the S/N-ratios are proportional to the ENDOR peak amplitude. The increment in ENDOR peak amplitudes due to the use of larger sample sizes (last column of Table 1) closely follows the increment found for the ESE amplitudes.

The TE_{102} rectangular cavity performance at T = 20 K is illustrated in Table 2 as a result from primary ESE and Davies ENDOR experiments in an aqueous solution of the transition metal complex bis(glycinato)copper(II) prepared with ^{63}Cu. Cryogenic temperatures allow for an increase of longitudinal and transversal

Table 1
Room temperature performance of the TE_{102} ENDOR resonator and dielectric ENDOR resonator. The experiments were performed with a coal sample.

Sample tube diameter (i.d. × o.d.) [mm × mm]	ν_{mw} [GHz]	ESE amplitude [mV]	Sensitivity factor Λ_{rs}[a] [mV/mm^3]	mw pulse power P_1[b] [mW]	Q_L[c]	mw pulse efficiency $\Lambda_{p(mw)}$[a] [T/√W]	ENDOR[d] amplitude [a.u.]
TE_{102} rectangular ENDOR resonator							
1.0 × 1.6	34.2	280	50	790	260	11×10^{-5}	4300
1.5 × 1.8	35.9	430	35	790	260	11×10^{-5}	6600
2.5 × 2.9	34.9	1500	42	790	260	11×10^{-5}	22000
DR-ENDOR resonator [e]							
1.0 × 1.6	34.6	440	112	63	400	39×10^{-5}	8500

The error in the estimation of the quantities given in this table can be up to 10%.
[a] Λ_{rs} = Echo intensity/sample volume; $\Lambda_{p(mw)} = B_1/\sqrt{P_1}$.
[b] The incident power P_1 is measured at constant receiver gain and bandwidth at the maximum of the echo amplitude using a coal sample with the sequence $\pi/2$-π-τ-echo ($t_{\pi/2}$ = 80 ns, t_π = 160 ns, τ = 300 ns).
[c] Q_L is the loaded quality factor that was measured for the TE_{102} ENDOR cavity with a calibrated network analyzer (hp 8722ES) at a coupling scattering parameter (S_{11}) from −15 to −25 dB with coal samples. For the overcoupled DR-ENDOR resonator, Q_L was estimated by the decay time constant of the reflected excitation pulses [26].
[d] The rf incident power was 500 W for the TE102 ENDOR resonator and 250 W for the DR-ENDOR resonator (maximum as specified by Bruker). For both resonators the optimum rf pulse length was found to be approx. 8500 ns by a rf-ENDOR nutation experiment.
[e] Bruker Biospin Q-band EN 5107D2 resonator for pulse EPR and ENDOR operating in the TE_{011} mode.

Table 2
Performance of the TE_{102} and DR-ENDOR resonators at cryogenic temperatures. The experiments were performed with a solution of 1.125 mM bis(glycinato)copper(II) (^{63}Cu) and 25 mM glycine in a 5:1 water/glycerol mixture, at 20 K.

Quartz tube diameter (i.d. × o.d.) [mm × mm]	ν_{mw} [GHz]	ESE amplitude [mV]	Sensitivity factor Λ_{rs}[a] [mV/mm^3]	rf pulse power P_i [W]	rf pulse power efficiency $\Lambda_{p(rf)}$ [T/√W]	ENDOR amplitude [a.u.]
TE_{102} rectangular ENDOR resonator						
1.0 × 1.6	34.35	100	18	500	6.2 10^{-5}	3300
1.5 × 1.8	36.01	136	11	500	6.2 10^{-5}	4500
2.5 × 2.9	34.51	320	9	500	6.2 10^{-5}	10000
DR-ENDOR resonator						
1.0 × 1.6	34.78	200	36	250[a]	8.7 10^{-5}	6000

[a] Maximum rf power according to Bruker specifications.

relaxation times T_1 and T_2, respectively, and lead to a more favorable Boltzmann distribution of the populated spin states, i.e. an increase of pulse EPR signal amplitudes.

The improvement of the ESE amplitudes by the use of larger samples is significantly smaller for the frozen aqueous solution at 20 K (Table 2) as compared to the ones obtained at room temperature for the coal sample (Table 1). The higher dielectric constant of the frozen solution results in a weaker B_1-field strength at the sample position (see electromagnetic simulations).

The rf pulse power efficiency $\Lambda_{p(rf)} = B_2/\sqrt{P_i}$ data collected in Table 2 were calculated using the length of the π rf pulse determined by an rf nutation experiment. $\Lambda_{p(rf)}$ in our TE_{102} ENDOR resonator remains the same for all sample sizes but it is considerably smaller than in the DR-ENDOR resonator. The lower $\Lambda_{p(rf)}$ is compensated by increasing the rf power through our more robust coils, resulting in the same rf pulse lengths for both resonators.

As compared to the ENDOR signal for quartz tubes of 1.0 mm i.d., the increase of the ENDOR signal by a factor of 1.4 for 1.5 mm i.d. sample tubes and by a factor of 3 for 2.5 mm i.d. tubes was comparable to the increase of the ESE signal. The comparison of the ENDOR peak amplitudes as acquired with the TE_{102} rectangular cavity and the DR-ENDOR resonator demonstrate the good performance of the DR-ENDOR resonator for small sample volumes (see Table 2). The measurement with a quartz tube with 2.5 mm × 2.9 mm in diameter, however, resulted in an ENDOR peak amplitude which is close to double compared with the DR resonator.

Data on the rf performance of the ENDOR coil at different frequencies are collected in Table 3. In the second column, the radio frequency B_2-field strengths are displayed. The values were calculated using the following expression:

$$B_2 = \sqrt{2}U_{rms}/2\pi\nu_{rf}An[V\mathrm{Hz}^{-1}\mathrm{m}^{-2}]$$

where U_{rms} was measured with a 2 turn 1 mm in diameter pick up coil placed in a sample tube in the middle of the ENDOR cavity resonator, ν_{rf} is the radio frequency. Here A is the area and n the number of turns of the pick up coil. The B_2-field was measured with an incident power of 10 mW and then scaled to the actual power, 500 W; subsequently, it was divided by two to compare with the values measured in the rotating frame using rf nutation experiments. Reasonable agreement was found between the two measurements. The B_2-field of the ENDOR coil shown in Table 3 was found to have a drop of about 6% over the frequency range ν_{rf} = 22.5–180 MHz.

In the 3rd column of Table 3 the scattering parameter S_{11} of the ENDOR rf broadband system measured with a network analyzer are displayed. $\Lambda_{p(rf)}$ is given for B_2-field estimations and the available rf power.

4. Electromagnetic field simulations

The use of large samples to improve the echo amplitude results in non-negligible electric fields in the sample volume. In spite of this unwanted effect, the cavity resonator performs well in ENDOR experiments as already described above. To better understand this apparent contradiction, information is required about:

- The distribution of mw fields and their perturbation by the ENDOR coil and by the dielectric properties of the quartz and the sample.
- The distribution of the rf magnetic field.

To obtain this information, field calculations were done with the commercial tool CST MICROWAVE STUDIO [27], which uses a volume grid discretization and the Finite Integration Technique (FIT). The complete structure including all coupling elements (iris, coupling rod and transition to waveguide) was modeled by roughly 65.000 Cartesian mesh cells for the mw field calculations and by additional 40.000 mesh cells for the calculation of the rf fields. In the most critical parts (sample area and ENDOR coil) the resolution was below 100 μm. All metal structures were calculated using a surface impedance model to incorporate resistive losses. The sample area was filled in the model with a quartz tube of diameter 2.9 mm (ε = 4.2) containing samples with a dielectric constant of either ε = 2.7, to model frozen aqueous solutions or ε = 1 for other, non-dielectric, samples. The value of 2.7 as an effective dielectric constant for ice at Q-band frequencies was estimated from the observed frequency shifts caused with the 2.5 × 2.9 mm quartz tube with the aqueous sample. The ENDOR coil was modeled as four silver wires crossing the resonator space very close to the sample and connected outside the resonator to form a loop.

The setup was analyzed by a two step procedure: first, the modeled structure was excited by a chirped Gaussian pulse containing the frequency range between 33 and 37 GHz. From the calculated transfer function (frequency analysis of the reflected power) the resonance frequency and the Q_L of the TE_{102} mode were obtained. The value of ν_0 = 34.70 GHz found in this calculation is in excellent agreement with the experimental values. A second run of simulations on the same grid model with the same excitation, this time using an additional field monitor at the resonance frequency, yielded the three dimensional distribution of the electromagnetic fields. The microwave field plots are shown in Figs. 2 and 3, where the field intensities were normalized to an incoming microwave power of 1 W.

Figs. 2a and b show a representation of the E_1-field z-component in a cross-section contained in the x–z plane using samples with ε = 2.7 and 1.0, respectively. The same magnitude is displayed in Fig. 2c and d in a cross-section within the x–y plane. In the Figures it can be observed that, as expected for the mode TE_{102} of a rectangular cavity, there is a large field gradient in the direction of the x-axis (each color step stands for 10% of the field intensity), the intensity of the electric field increases rapidly when moving away of the center of the cavity, where its value is zero, and can attain 10^4 V/m (65% of its maximum value) in a small outer region of the sample volume. E_1-fields in the sample region are generally to be avoided as they eventually create heat and lead to a decrease in Q_L. Although the differences in E_1-field distribution in the two different samples are minimal, there is a slight pull-in effect of the E_1-field into the sample region of a higher dielectric constant. This effect is similar to the one produced by sample holders, which can change the field distributions, as has been already reported for flat sample cells [28,29].

Fig. 2c and d nicely illustrate the sine wave of the TE_{102} mode inside the cavity with the maximal E_1-field located at the iris.

The representation of the microwave B_1-field strength distribution in three perpendicular cross-sections is displayed in Fig. 3 for the two kinds of samples studied. The mw magnetic field, which is directed along the y-axis, is maximal and fairly homogeneous at the center of the cavity but decreases on going up and down along the y-axis until it drops to almost zero at the top and bottom of the

Table 3
B_2-field strength, scattering parameter, S_{11}, and rf pulse efficiency $\Lambda_{p(rf)}$ of the four-wire rf-coil in the TE_{102} resonator operating at 22.5–180 MHz.

ν_{rf} [MHz]	$B_2[10^{-4}$ T]	S_{11} [dB][a]	$\Lambda_{p(rf)}$ [T/√W]
22.5	11.1	−25	5.0 10^{-5}
45	11.0	−20	4.9 10^{-5}
90	10.7	−14	4.8 10^{-5}
180	10.4	−9.3	4.6 10^{-5}

[a] Values measured with an Agilent RF Network analyzer 8714ES.

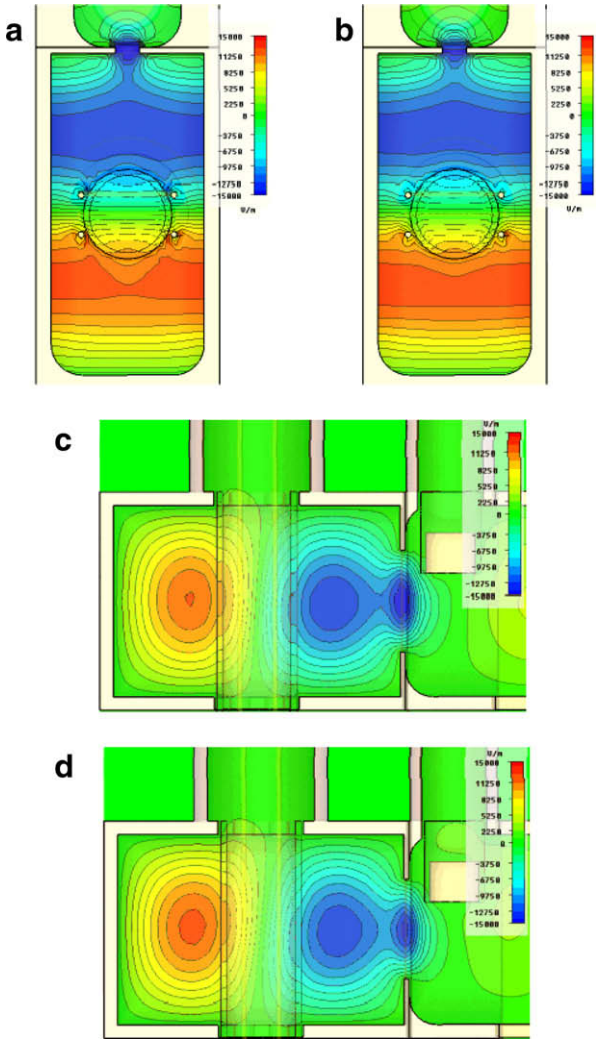

Fig. 2. Calculation of the E_1-field along the z-component in a cross-section contained in the x–z plane; (a) sample with $\varepsilon = 2.7$, (b) sample with $\varepsilon = 1$. Calculation of the E_1-field along the z-component in a cross-section contained in the x–y plane; (c) sample with $\varepsilon = 2.7$, (d) sample with $\varepsilon = 1$.

cavity. Nevertheless, 50% of the sample volume is located in the region where the B_1-field is within 20% of its maximum value.

As the structure is not resonant for the rf, the B_2-field distribution generated by the ENDOR coil was calculated as the response to a Gaussian excitation in the loop covering the range between 50 and 100 MHz, with a field monitor at 60 MHz. The results of the calculations are shown in Fig. 4. In the cross-sections perpendicular to the sample axis it can be observed that the maximum intensity is produced in a small region very close to the silver wires, B_2 drops then to about 60% of its maximum value but is homogeneous in the center of the sample. From Fig 4c one can appreciate that the B_2-field homogeneity is very good along the axis of the sample (y-axis). It has to be noted that the central region, where the B_2-field is homogenous, overlaps with the area of maximal and homogenous B_1-fields. If according to Fig. 3 we calculate the area where the B_1-field irradiation is within 10% of the maximum value, we obtain an approximate value of 10 µl. In view of the B_2-field calculations, only about 60% of the cross-section of the tube is homogenously irradiated (within 10% of the maximum value). This result in about 6 µl of sample volume with both, strong mw pulses producing intense electron spin echoes and also homogenous rf irradiation which drives the nuclear transitions and produces the ENDOR signals. Compared to an assumedly homogeneously irradiated 1.6 mm tube with 1 mm inner diameter, this results in an approximately three fold increase in contributing volume, in good agreement with the ESE and ENDOR intensity results presented in the previous section.

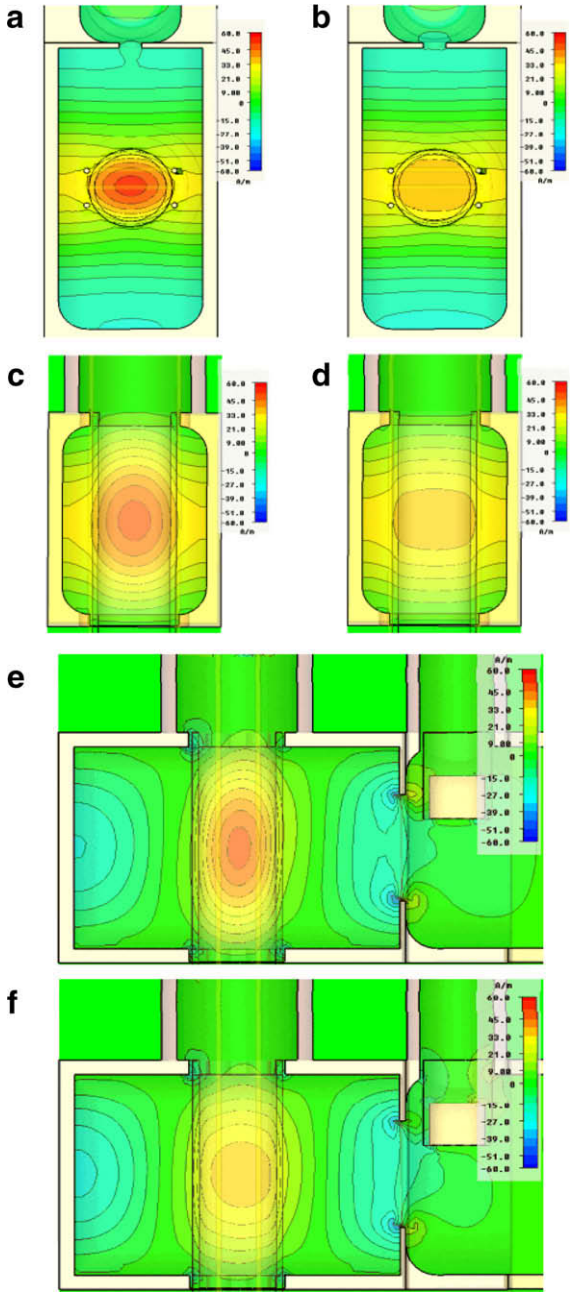

Fig. 3. Calculated B_1-field strength distribution. Cross-section in the x–z plane with sample $\varepsilon = 2.7$ (a) and $\varepsilon = 1$ (b). Cross-section in the y–z plane, $\varepsilon = 2.7$ (c); $\varepsilon = 1$ (d). Cross-section in the x–y plane, $\varepsilon = 2.7$ (e); $\varepsilon = 1$ (f).

5. Applications

Pulsed EPR and ENDOR are widely used to determine the electronic and geometric structure of paramagnetic species, as these techniques provide hyperfine and quadrupole couplings of nuclear spins in the molecular environment of unpaired electrons. To demonstrate the performance of the TE_{102} ENDOR resonant cavity for oversized samples, we present some experimental results on

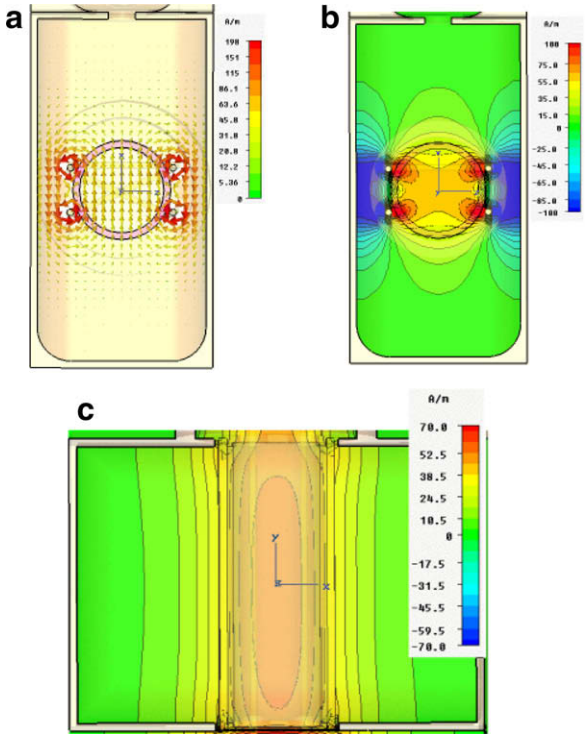

Fig. 4. (a) Vector representation of the B_2-field distribution in the x–z plane. (b) B_2-field intensity distribution in the y–z and (c) in the x–y plane. The field change between contour lines is 10%.

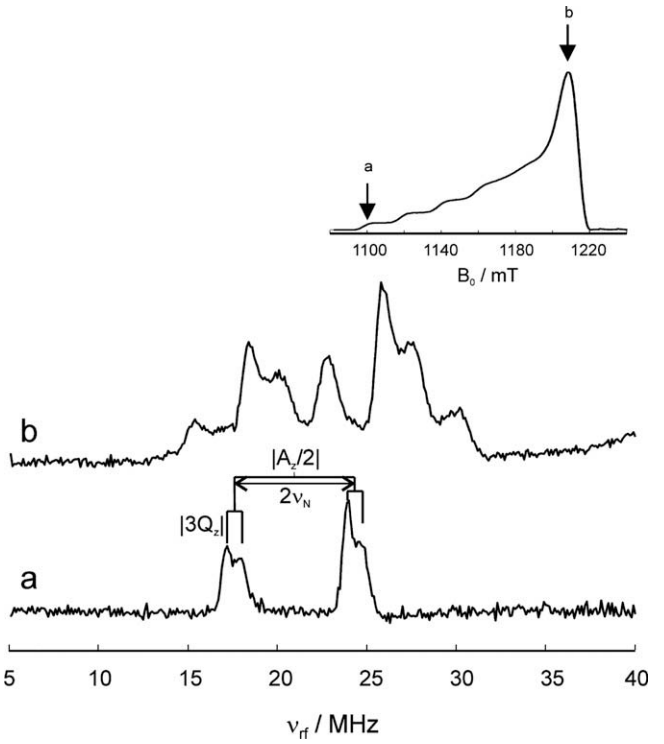

Fig. 5. Davies ENDOR spectra of Cu(II) 2,9,16,23-tetra-*tert*-butyl-29H,31H-phthalocyanine in sulfuric acid measured at $T = 20$ K at the field positions (a) $B_0 = 1101$ mT ($g_{||}$), (b) $B_0 = 1209$ mT (g). The sequence, π-π_{rf}-$\pi/2$-τ-π-echo, used $t_{\pi/2,\,\pi} = 20$, 40 ns, $\tau = 300$ ns and $t_{rf} = 14$ μs. Inset: echo-detected EPR spectrum of the complex using the sequence $\pi/2$-τ-π-echo with $t_{\pi/2} = 16$ ns, $t_{\pi} = 32$ ns and $\tau = 300$ ns. The arrows indicate the field positions where the two ENDOR spectra were acquired.

systems that are typical for applications on metalloproteins and catalyst materials.

5.1. Strongly coupled nitrogen nuclei of Cu–phthalocyanine

Resolved ENDOR spectra of nuclei with low gyromagnetic ratios nuclei such as ^{2}H, ^{13}C, and ^{14}N are difficult to obtain at X-band since the spectral region can be very cluttered. Often strongly coupled ^{14}N nuclei ($A \sim 30$ MHz) overlap with the proton signals centered on ca. 15 MHz.

Fig. 5 shows the performance of the TE_{102} resonator to measure the magnetic couplings of the directly coordinated nitrogens in the complex Cu–phthalocyanine. The phthalocyanines (a synthetic analog of the porphyrin macrocycle) and metal phthalocyanines (MPc) are used in industry in a variety of applications ranging from conventional dyes to catalysis, or from coatings for read/write compact discs to anti-cancer agents. Due to their photocatalytic activities these compounds are also applied as oxidation–reduction catalysts. For the design of new MPc materials it is important to evaluate the effect of the substituents of the macrocycle and the solvents on the spin density distribution of the complex, which influences its catalytic activity [30].

Q-band Davies ENDOR experiments are very well suited for determining the strong hyperfine coupling of the directly coordinated isoindole nitrogens since the proton signals (centered around ca. 55 MHz) are well separated from the ^{14}N signals. The ^{14}N ENDOR spectra are characterized by peaks centered at approximately half of the hyperfine splitting $|A/2|$ and split by twice the nitrogen nuclear Zeeman frequency, $2\nu_N$. Additional further splitting results from the nuclear quadrupole interaction (of $3Q$). A further advantage of using this microwave frequency is that the different nuclear transitions are well separated as the condition $A > 2\ \nu_N > 3Q$ is fulfilled, which allows a straight forward assignment of the different nuclear frequencies.

5.2. Weakly coupled proton nuclei of Co-porphyrin complexes

Hemoglobin (Hb) and myoglobin (Mb) are dioxygen binding heme proteins. In the active form, the prosthetic heme iron is in the reduced state which is EPR silent. The electronic structure of these proteins can be investigated by EPR after replacing the iron(II) ion by cobalt(II). Recently dioxygen adducts of Co-Mb and cobalt-containing model compounds for Mb and Hb were studied

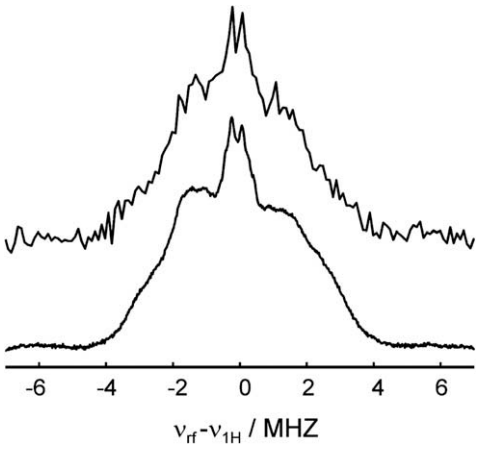

Fig. 6. Q-band Davies ENDOR spectra of model complex 1-Co-O_2 for Mb; *upper trace*: experiment performed with standard Q-band resonator and o.d. sample tube 1.6 mm, *lower trace*: experiment performed with the TE_{102} resonator and o.d. sample tube 2.9 mm. The measuring time was the same for both spectra. $B_0 = 1230$ mT, $\nu_{mw} = 34.6$ GHz.

in our laboratories. The proton hyperfine couplings were examined with the main emphasis on distal hydrogen bonding [31,32].

Due to the cross-suppression effect, which hampers the determination of shallow modulation, the proton hyperfine couplings initially could not be detected at X-band [11,33,34]. Q-band Davies ENDOR experiments later allowed for the detection of the complete proton signals revealing the hyperfine couplings. However, the S/N-ratio was low because of the significantly reduced sample size (sample tube o.d. 1.6 mm) for standard Q-band resonators (see Fig. 6). By using oversized samples (o.d. 2.9 mm) in the TE_{102} ENDOR resonator we achieved a significantly higher S/N-ratio. The increase in signal intensity was crucial for the detection of the weak and broad part of the spectrum.

The enhanced ESE signal also permitted two-dimensional experiments within reasonable time. The 2.9 mm o.d. sample tubes containing these valuable samples could also be used at X-band frequencies where the satisfying filling factor easily allowed for recording two-dimensional ESEEM spectra. In addition, the larger sample tubes allowed for an easier preparation of the samples because the delicate dioxygen adduct formation could now be done directly inside the Q-band sample tube.

6. Conclusions

In contrast to LGR and DR, the TE_{102} ENDOR cavity resonator allows for Q-band ENDOR experiments with oversized 2.5×2.9 mm sample tubes, as they are used for pulse EPR at 9–10 GHz frequencies. Experimental tests reveal a good ESE sensitivity, high Q_L and filling factor as well as a nearly constant RF pulse efficiency in the range 22–180 MHz. Electromagnetic field calculations for the first time give detailed information of the influence of a frozen aqueous sample with dielectric constant $\varepsilon \approx 2.7$ at 20 K and a sample with $\varepsilon = 1$ at 290 K on the B_1- and B_2-field homogeneities and the E_1-field strength in the sample volume. An improvement in the signal-to-noise ratio at given concentration of paramagnetic centers with respect to standard 1.0×1.6 mm i.d. sample size resonators is demonstrated in the experimental spectra of two transition metal complexes.

Acknowledgments

This work has been supported by ETH Zurich, the Swiss National Foundation and NCCR Nanoscale Science. We acknowledge M. Hausmmann for his skilled electro spark work and support for the fabrication process of the resonant cavity. We thank P. Müller (from Collini Fluehmann AG) for the high quality silver plating of the cavity. With deep sorrow we thank and remember here Prof. Arthur Schweiger who enthusiastically supported the ideas that lead to this work.

References

[1] E.R. Davies, A new pulse ENDOR technique, Phys. Lett. 47A (1974) 1–2.
[2] W.B. Mims, Pulsed Endor experiments, Proc. R. Soc. Lond. 283 (1965) 452–457.
[3] M. Dorio, J.H. Freed, Multiple Electron Resonance Spectroscopy, Plenum, New York, 1979.
[4] A. Schweiger, Electron Nuclear Double Resonance of Transition Metal Complexes with Organic Ligands, Springer, Berlin, 1982.
[5] C. Gemperle, A. Schweiger, Pulsed electron-nuclear double resonance methodology, Chem. Rev. 91 (1991) 1481–1505.
[6] A. Schweiger, G. Jeschke, Principles of Pulse Electron Paramagnetic Resonance, Oxford University Press, Oxford, 2001.
[7] B. Epel, D. Arieli, D. Baute, D. Goldfarb, Improving W-band pulsed ENDOR sensitivity-random acquisition and pulsed special TRIPLE, J. Magn. Reson. 164 (2003) 78–83.
[8] Gromov, J. Forrer, A. Schweiger, Probehead operating at 35 GHz for continuous wave and pulse electron paramagnetic resonance applications, Rev. Sci. Instrum. 77 (2006) Art. No. 064704.
[9] W. Bruggemann, J.R. Niklas, Stochastic Endor, J. Magn. Reson. A 108 (1994) 25–29.
[10] P.E. Doan, M.J. Nelson, H.Y. Jin, B.M. Hoffmann, An implicit TRIPLE effect in Mims pulsed ENDOR: a sensitive new technique for determining signs of hyperfine couplings, J. Am. Chem. Soc. 118 (1996) 7014–7015.
[11] S. Stoll, C. Calle, G. Mitrikas, A. Schweiger, Peak suppression in ESEEM spectra of multinuclear spin systems, J. Magn. Reson. 177 (2005) 93–101.
[12] J. Forrer, I. Garcia-Rubio, R. Schuhmann, R. Tschaggelar, J. Harmer, Cryogenic Q-band (35 GHz) probehead featuring large excitation microwave fields for pulse and continuous wave electron paramagnetic resonance spectroscopy: performance and applications, J. Magn. Reson. 190 (2008) 280–291.
[13] J. Hoentsch, Y. Rosentzeig, D. Heinhold, K. Köhler, M. Gutjahr, A. Pöppl, G. Völkel, R. Böttcher, A Q-band pulsed ENDOR spectrometer for the study of transition metal ion complexes in solids, Appl. Mag. Reson. 25 (2003) 249–259.
[14] C.E. Davoust, P.E. Doan, B.M. Hoffman, Q-band pulsed electron spin-echo spectrometer and its application to ENDOR and ESEEM, J. Magn. Reson. A 119 (1996) 38–44.
[15] A.V. Astashkin, J.H. Enemark, A. Raitsimring, 26.5–40 GHz Ka-band pulsed EPR spectrometer, Concepts Magn. Reson. B Mag. Res. Eng. 29B (2006) 125–136.
[16] C.P. Poole, Electron Spin Resonance, second ed., Dover, New York, 1983.
[17] R. Böttcher, D. Heinhold, An X-band cavity for electron-nuclear triple resonance experiments in solids, Exp. Techn. Phys. 34 (1986) 87–94.
[18] H.L. Vancamp, C.P. Scholes, R.A. Isaacson, Plastic Endor cavity for studies of biological compounds at 2k, Rev. Sci. Instrum. 47 (1976) 516–517.
[19] G. Feher, Electron spin resonance experiments on donors in silicon.1. Electronic structure of donors by the electron nuclear double resonance technique, Phys. Rev. 114 (1959) 1219–1244.
[20] R.C. Rempel, C.E. Ward, R.T. Sullivan, M.W. Clair St., H.E. Weaver, Gyromagnetic resonance method and apparatus, U.S. Patent No. 3 122 703, February 25, 1964, Varian Associates, USA, 1964.
[21] R. Biehl, The dielectric ring TE011 cavity, Bruker Rep. 1 (1986) 45.
[22] J. Forrer, S. Pfenninger, A. Schweiger, T. Weiland, Bridged-Loop-Gap and Dielectric Resonators for Pulsed ESR and ENDOR Spectroscopy with Light Excitation, Magnetic Resonance and Related Phenomena, Elsevier, 1989.
[23] I. Gromov, J. Shane, J. Forrer, R. Rakhmatoullin, Y. Rozentzwaig, A. Schweiger, A Q-band pulse EPR/ENDOR spectrometer and the implementation of advanced one- and two-dimensional pulse EPR methodology, J. Magn. Reson. 149 (2001) 196–203.
[24] K.P. Dinse, R. Biehl, K. Mobius, Electron nuclear triple resonance of free-radicals in solution, J. Chem. Phys. 61 (1974) 4335–4341.
[25] J. Forrer, S. Pfenninger, J. Eisenegger, A. Schweiger, A pulsed ENDOR probehead with the bridged loop-gap resonator, construction and performance, Rev. Sci. Instrum. 61 (1990) 3360–3367.
[26] M. Willer, J. Forrer, J. Keller, S. Van Doorslaer, A. Schweiger, R. Schuhmann, T. Weiland, S-band (2–4 GHz) pulse electron paramagnetic resonance spectrometer: Construction, probe head design, and performance, Rev. Sci. Instrum. 71 (2000) 2807–2817.
[27] CST Microwave Studio: CST GmbH, Darmstadt, Germany. Available from: <www.cst.com>.
[28] J.S. Hyde, A new principle for aqueous sample cells for EPR, Rev. Sci. Instrum. 43 (1972) 629–631.
[29] J.W. Sidabras, R.R. Mett, J.S. Hyde, Aqueous flat-cells perpendicular to the electric field for use in electron paramagnetic resonance spectroscopy, II: design, J. Magn. Reson. 172 (2005) 333–341.
[30] C. Finazzo, C. Calle, S. Stoll, S. Van Doorslaer, A. Schweiger, Matrix effects on copper(II)phthalocyanine complexes. A combined continuous wave and pulse EPR and DFT study, Phys. Chem. Chem. Phys. 8 (2006) 1942–1953.
[31] H. Dube, B. Kasumaj, C. Calle, B. Felber, M. Saito, G. Jeschke, F. Diedrich, Probing hydrogen bonding to bound dioxygen in synthetic models heme proteins: the importance of precise geometry, Chem. Eur. J. 15 (2009) 125–135.
[32] H. Dube, B. Kasumaj, C. Calle, M. Saito, G. Jeschke, F. Diederich, Direct evidence for a hydrogen bond to bound dioxygen in a myoglobin/hemoglobin model system and in cobalt myoglobin by pulse EPR spectroscopy, Angew. Chem. Int. Ed. 47 (2008) 2600–2603.
[33] C. Calle, Continuous wave and pulse EPR investigation of novel copper(II) and cobalt(II) containing complex, Diss. ETH No. 16883 (2006).
[34] B. Kasumaj, S. Stoll, 5- and 6-Pulse electron spin echo envelope modulation (ESEEM) of multi-nuclear spin systems, J. Magn. Reson. 190 (2008) 233–247.